9-15-2000

Analysis of the NiCo$_2$O$_4$ spinel surface with Auger and X-ray photoelectron spectroscopy

J.-G. Kim
University of Nebraska - Lincoln

D. L. Pugmire
University of Nebraska - Lincoln

D. Battaglia
University of Nebraska - Lincoln

Marjorie Langell
University of Nebraska - Lincoln, mlangell1@unl.edu

Analysis of the NiCo$_2$O$_4$ spinel surface with Auger and X-ray photoelectron spectroscopy

J. -G. Kim, D. L. Pugmire, D. Battaglia and M. A. Langell*

Department of Chemistry, University of Nebraska–Lincoln, Lincoln, NE 68588-0304

* Corresponding author. Email: mlangell@unlserve.unl.edu

Abstract: Nickel cobaltite, NiCo$_2$O$_4$, has been synthesized by sol–gel and thermal decomposition techniques and the surface composition studied with Auger (AES) and X-ray photoelectron spectroscopies (XPS). The as-introduced samples are near-stoichiometric, although samples fabricated by thermal decomposition tend to be oxygen-deficient by approximately 25% of the predicted spinel concentration. Nickel 2p XPS indicates the predominant form of the metal to be Ni^{2+}, with the cations located in octahedral sites. The cobalt cations are equally divided between tetrahedral and octahedral sites as Co^{3+}. The oxygen XP 1s spectrum is composed of two peaks, the main lattice peak at 529.6 eV and a component at 531.2 eV with about 40% of the total O 1s intensity in stoichiometric samples. While the possibility of hydroxyl contaminants cannot be discounted, most of the intensity in the 531.2 eV peak is believed to be intrinsic to the NiCo$_2$O$_4$ surface. Heating the cobaltite in ultrahigh vacuum (UHV) results in surface reduction, with the largest changes apparent in the Co 2p XP spectrum, which shows clear signs of reduction to octahedral Co^{2+}. Changes brought about by the reduction are not reversible, and although it is possible to reoxidize the material, the surface undergoes phase separation to Co$_3$O$_4$ and Ni$_x$Co$_{1-x}$O.

Keywords: Oxides, Solid solutions, Cobalt oxide, Nickel oxide, Defects

1. Introduction

Transition metal oxides have a host of useful chemical, electronic and magnetic properties, many of which are relevant to surface-related applications. Nickel cobaltite, NiCo$_2$O$_4$, is a mixed-metal oxide spinel that has shown exceptional ability to serve as an oxygen evolution electrode and has been studied quite extensively by electrochemical methods for this purpose [1, 2]. The material also possesses interesting magnetic properties and has been shown to be ferrimagnetic with a Curie temperature, T_C of approximately 400°C [3].

The generic spinel structure is formed from a face-centered cubic close packing of O^{2-} anions, with one half of the octahedral sites and one eighth of the tetrahedral sites created by the O^{2-} lattice filled with cations. To preserve charge neutrality, one-third of the cations are formally in the oxidation state of 2+ and

the remaining two-thirds are found as 3+ cations. However, the actual cation charge and site distribution is specific to the compound of interest. The bulk structure of nickel cobaltite has been studied by a combination of magnetization, X-ray, neutron diffraction and ^{61}Ni Mössbauer spectroscopic techniques [4–9] and, while all studies agree that the bulk nickel cations are essentially exclusive in their occupation of octahedral sites, assignment of the charge distribution among the nickel, octahedrally located cobalt and tetrahedrally located cobalt is not as straightforward. Whether it results from differences in sample preparation or uncertainty inherent in the measurement techniques, or both, oxidation state distributions have been reported for nickel cobaltite that are highly variable and cover the entire range of $Co_{1-x}^{2+}Co_x^{3+}[Co^{3+}Ni_x^{2+}Ni_{1-x}^{3+}]O_4$, $0 \leq x \leq 1$. In this formalism, cations preceding the brackets are taken to be in tetrahedral sites and those within the brackets are in octahedral sites.

The surface composition of nickel cobaltite has also been studied, primarily by X-ray photoelectron spectroscopy (XPS) with a focus on the binding energies and peak shapes of the nickel and cobalt 2p core level photoemission features [10–14]. The reported results vary in part due to individual interpretations of the peak structure but potentially also due to differences in sample preparation and surface pretreatment. Two nickel species, with variable relative XPS 2p intensities, have been identified in the surface studies. The lower binding energy species (2p$_{3/2}$ 853.5–854.9 eV) is generally predominant in the spectrum and has binding energies comparable in value to that of Ni^{2+} in NiO. This assignment is not controversial, although the wide range in binding energies reported for the species indicates difficulties with calibration procedures or other problems in some of the studies.

The origin of the higher binding energy peak (855.6–856.2 eV) is, however, less certain. The peak is quite variable in intensity and in some cases represents the majority nickel species present at the surface. It has been reported as intrinsic to the NiCo$_2$O$_4$ surface and to result from Ni^{3+} located in octahedral sites of the spinel structure in coexistence with the Ni^{2+} species described above [10]. Charge neutrality then dictates that the cobalt cations, presumably divided equally between tetrahedral sites and the remaining octahedral sites of the lat-

tice, form one Co^{2+} to compensate for every Ni^{3+} with the remaining cobalt in the 3+ oxidation state. In other studies, the higher binding energy nickel peak was postulated to result not from an intrinsic nickel species but from surface hydroxylation and/or oxyhydroxide formation, perhaps accompanied by phase separation from the NiCo$_2$O$_4$ remaining at the surface [11–14]. All of these studies have relied on curve-fitting procedures to separate the overlapping, multi-peaked 2p XPS structure of the two metal oxidation states.

We present here the surface analysis of NiCo$_2$O$_4$ prepared by two different solid state synthetic methods, thermal decomposition of nickel and cobalt nitrates mixed in appropriate stoichiometric amounts [4] and a sol–gel route [15]. Several different sample treatment conditions were also employed. The bulk structure was found to be homogeneous NiCo$_2$O$_4$ by X-ray diffraction (XRD) and surface analysis was carried out using Auger (AES) and X-ray photoelectron (XPS) spectroscopies. Surface concentrations were stoichiometric or near-stoichiometric, although the thermal decomposition route tended to produce samples that are slightly deficient in oxygen. Reduced surfaces are more active than as-synthesized, stoichiometric NiCo$_2$O$_4$, and these materials show evidence of phase separation upon re-oxidation.

2. Experimental

Cobalt (II) nitrate hexahydrate (98% purity) and nickel (II) nitrate hexahydrate (99.999% purity) were obtained from Aldrich Chemical and were used without further purification. In the thermal decomposition method, stoichiometric amounts of the cobalt and nickel nitrates were weighed out under dry, oxygen-free glove box conditions, intimately ground with a mortar and pestle and the mixture heated under flowing, dry air for 4 h at 573 K. Here, and in subsequent citations, dry air specifically refers to Air Products UHP Zerograde air certified to contain less than 0.5 ppm hydrocarbons and 3.5 ppm H$_2$O. The resulting powder NiCo$_2$O$_4$ sample was cooled under flowing dry air and stored under dry N$_2$ until needed.

NiCo$_2$O$_4$ was also synthesized by a sol–gel method [15]. Equal volumes of aqueous 0.50 M nickel nitrate and 1.00 M cobalt nitrate were mixed thoroughly and

precipitated as carbonates. After vacuum filtration, the carbonate mixture was dissolved in excess propanoic acid (approximately 150 ml solvent to 100 g carbonate mixture) and the excess solvent was slowly evaporated at 413 K until a violet, translucent gel formed. The gel was cooled to room temperature and powdered by the addition of liquid nitrogen to aid in transferring the sample to a porcelain boat, where the powder was heated under flowing dry air at 453 K for 24 h and then at 573 K for 3 h. The sample was cooled under flowing, dry air and stored under dry N_2 until needed.

Because of the differences in chemical species involved in the two synthetic procedures, it is not straightforward to compare severity of reaction conditions simply by matching final temperatures and length of heating. The temperatures and times for the sold state syntheses were chosen, with consideration given to those cited in published, successful synthetic methods, to give complete transformation to nickel cobaltite in the bulk with the least severe conditions possible. Temperatures as low as 723 K have been shown to lead to bulk decomposition and/or significant deviations from non-stoichiometry. Similar decomposition temperatures are found for surface compositions, as described more extensively in Section 3.3 below. The homogeneity and bulk stoichiometry of the two samples were determined with powder XRD using a Rigaku Geigerflex diffractometer equipped with a Cu Kα anode. Diffraction features were sharp and agree in position and relative intensity with previously published XRD data [15]. No phase separation was observed in the bulk and no NiO, CoO, Co_3O_4 or any of their hydroxides were detected by XRD.

The $NiCo_2O_4$ samples were introduced into an ultrahigh vacuum (UHV) surface analysis chamber through a rapid transfer load-lock system. The UHV chamber was equipped with both ion and turbo pumps for a total pumping speed of 480 l/s on a bell jar volume of approximately 40 l, and routinely operated at a base pressure of $\lesssim 3 \times 10^{-10}$ Torr. This arrangement obviated the need for a bake-out and surface analysis could begin within minutes of insertion into UHV. It was not possible to prevent exposure of the $NiCo_2O_4$ sample to laboratory ambient, however, and it is estimated that the total exposure time to ambient was approximately 15 min. For mounting in UHV, the powder sample was pressed into a piece of thin gold foil, which served to support the

sample and minimized charging in AES and XPS analyses. While this also provided a reference for XPS calibration through the Au $4f_{7/2}$ peak at 83.8 eV, we found it more accurate to use the lattice O 1s peak at 529.6 eV as an internal standard in the powdered material.

The sample could be heated by passing current through two tantalum wires between which the gold foil was suspended and the temperature of the foil was determined with a chromel–alumel thermocouple spot welded to the back of the foil. Since the $NiCo_2O_4$ coating on the oxide foil was fairly thin, the temperature of the foil was taken as a good approximation of the $NiCo_2O_4$ sample.

AES and XPS surface analysis was performed with a Physical Electronics 15-255G double-pass cylindrical mirror analyzer. AES was taken in a lock-in derivative mode with a 2-keV primary beam energy, a scan rate of 1.0 eV/s, a modulation energy of 2 eV and a time constant of 0.1 s. The AES spectra were signal averaged for 10 scans. XPS was obtained in a pulse-count mode at a constant pass energy of 25 eV. Photoemission was initiated with Mg Kα radiation (hv = 1253.6 eV) and the spectra, taken in increments of 0.1 eV with dwell times of 50 ms, were signal averaged for at least 100 scans. No decomposition or other changes were observed during the course of data acquisition.

3. Results

3.1. Auger analysis

Both thermal decomposition and sol–gel methods of synthesis yielded material that was bulk-homogeneous $NiCo_2O_4$, as determined by powder XRD methods. Although sol–gel methods have generally been reported to result in a higher surface area powder than is typical for thermal decomposition [15], both synthetic routes lead to qualitatively similar Auger spectra (Figure 1), with carbon the most common impurity. The grain size of the powders is typically reported to be on the order of microns, while the sampling depth in the surface analysis is approximately 50–100 Å, depending upon the kinetic energy of the Auger or X-ray photoelectron, so that observed differences or similarities in surface concentration reflect actual concentration profiles and are not artifacts of the measurement.
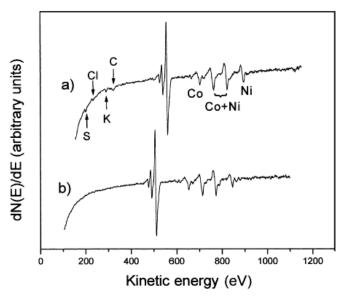
Figure 1. Auger spectra for typical NiCo$_2$O$_4$ samples synthesized by (a) thermal decomposition and (b) sol–gel methods. Trace (a) has been offset along the ordinate by 100 eV for clarity.

Small amounts of sulfur, chlorine and potassium were also observed. The impurities are very superficial and are estimated to be present in submonolayer quantities by their peak-to-peak Auger intensities. Ar$^+$ sputtering could eliminate the majority of these impurities after fluences of only 10^{16} Ar$^+$/cm^2 while otherwise leaving Auger and XP spectral characteristics unaffected. Note that many oxides are known to sputter incongruently to lose oxygen and, therefore, intensity analyses reported below rely on unsputtered samples unless otherwise noted. The carbon was primarily in the form of graphitic carbon, with XPS C 1s binding energies of 284.6 eV and with no carbide or carbonate detected.

The Auger data can be used to quantify the fractional nickel surface composition by use of Auger intensity values (I_i) and appropriate sensitivity factors (S_i):

$$x_{surface} = \frac{\dfrac{I_{Ni}}{S_{Ni}}}{\dfrac{I_{Ni}}{S_{Ni}} + \dfrac{I_{Co}}{S_{Co}}}. \tag{1}$$

Because the cobalt and nickel Auger transitions overlap significantly, the spectrum must first be integrated to ob-

tain the N(E) vs. E Auger spectrum and the individual nickel and cobalt components separated to obtain the integrated Auger intensity for each element independently. This procedure, which utilizes the overlapping Co L$_3$M$_{2,3}$M$_{2,3}$ and Ni L$_3$M$_{2,3}$V transitions, at 775 and 783 eV, respectively, and the non-overlapping Ni L$_3$M$_{2,3}$M$_{2,3}$ transition at 848 eV, is described in greater detail in [16]. S_{Ni} and S_{Co} values of 1.12 and 1.36 were found by procedures outlined in [17 and 18], and their use reproduces integrated Auger intensities for nickel and cobalt oxides quite well [16 and 19]. Note that Eq. (1) assumes that the compositional profile for the elements is uniform over the Auger sampling depth. The relative composition of the two metals is independent of the manner of preparation and the mean value obtained is $x_{surface}$ = 0.34 ± 0.04. As long as the bulk material was observed to be homogeneous and stoichiometric NiCo$_2$O$_4$, the surface fraction of nickel metal was also found to be within error of that expected from the bulk stoichiometry (x_{bulk} = 1/3). Mild sputtering (1 ≈ amp Ar$^+$ at 2 keV for 10 min) did not change $x_{surface}$ measurably.

The relative surface oxygen to total metal concentration, $C_O/C_{Ni}+C_{Co}$, can also be estimated from Auger intensity data:

$$\frac{C_O}{C_{Ni} + C_{Co}} = \frac{\dfrac{I_O}{S_O}}{\dfrac{I_{Ni}}{S_{Ni}} + \dfrac{I_{Co}}{S_{Co}}} \tag{2}$$

where the Auger sensitivity factor for the KL$_2$L$_2$ oxygen is S_O = 1.35 [16]. Samples prepared by thermal decomposition and sol–gel methods yield significantly different oxygen surface composition. Sol–gel surfaces give $C_O/C_{Ni} + C_{Co}$ = 1.49 ± 0.20, which is within error of that expected for a spinel sample ($C_O/C_{Ni} + C_{Co}$ = 1.33). Samples prepared by thermal decomposition yield $C_O/C_{Ni} + C_{Co}$ = 1.01 ± 0.06, indicating the surface obtained from thermal decomposition is somewhat reduced and has an oxygen surface concentration much closer to that expected for a metal monoxide. Errors are taken from the standard deviation, estimated from 10 or more measurements, and are at a 95% confidence level.
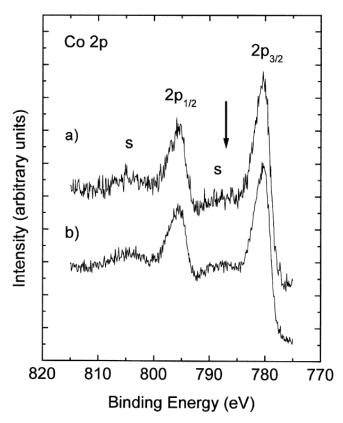
Figure 2. Cobalt 2p XPS for (a) thermal decomposition and (b) sol–gel methods. The arrow indicates the approximate position of the satellite characteristic of octahedral Co^{2+}, which is absent in the present spectra.

Figure 3. Comparison of cobalt 2p regions for $NiCo_2O_4$, Co_3O_4 and CoO(100). The $NiCo_2O_4$ sample is a powder synthesized by the thermal decomposition method; the Co_3O_4 and CoO are single crystal samples cleaved or crushed in UHV.

3.2. XPS analysis

Stoichiometric information can also be obtained from core photoemission intensity data. Values of $x_{surface}$ were calculated using Eq. (1) and the integrated intensities of the nickel 2p and cobalt 2p transitions, but with appropriate sensitivity factors for XPS data taken with a double pass cylindrical mirror analyzer and Mg Kα radiation. Values, which assume that the entire $2p_{3/2}+2p_{1/2}$ region has been integrated, are $S_{Ni} = 4.5$ and $S_{Co} = 3.8$ [20]. For XPS data, $x_{surface} = 0.39 \pm 0.07$, in agreement with both bulk composition and the surface composition obtained by AES above.

In addition to compositional information, XPS data also provide information on the chemical state of the elements in the near-surface region. The cobalt 2p binding energies and peak shape are similar for the two preparations (Figure 2) and yield binding energies of 780.1 and 795.2 eV for the $2p_{3/2}$ and $2p_{1/2}$ transitions, respectively. Unfortunately, the absolute binding energy of the $2p_{3/2}$ peak is not always very helpful in identifying the cobalt
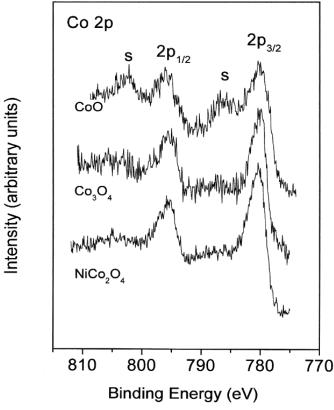
chemical environment, since relatively small shifts are reported to accompany oxidation of Co^{2+} to Co^{3+} [20–24]. However, the $2p_{3/2}$ to $2p_{1/2}$ separation and satellite structure have elements that are useful in characterizing the cobalt chemical environment.

Octahedral Co^{2+} cations, as found in CoO for example, have a very intense, characteristic satellite at ~787 eV, the approximate position of which is indicated by the arrow of Figure 2, and is shown explicitly for UHV-cleaved CoO(100) in Figure 3, where XP spectra for the 2p region are compared for the single crystal CoO(100), single crystal UHV-cleaved Co_3O_4 and a representative powder $NiCo_2O_4$ sample. Multiplet splitting causes extensive broadening in the CoO 2p spectrum, so that despite the fact that the monoxide has a single type of cobalt (octahedral Co^{2+}), its $2p_{3/2}$ spectrum is actually broader than that of $NiCo_2O_4$ and Co_3O_4, the latter of which is known to have two types of cobalt (tetrahedral Co^{2+} and octahedral Co^{3+}) contributing to this spectral region. For the data in Figure 3, the FWHM of the $2p_{3/2}$ main peak is measured as 4.0, 3.3 and ~6 eV for

$NiCo_2O_4$, Co_3O_4 and CoO, respectively. In the $NiCo_2O_4$ data, the relatively narrow peak width, the $2p_{3/2}$ to $2p_{1/2}$ separation of 15.1 eV and the very flat, weak satellite structure found to the high binding energy side of the $2p_{3/2}$ and $2p_{1/2}$ transitions indicate that few Co^{2+} cations occupy octahedral sites in the $NiCo_2O_4$ spinel lattice and that the majority of cobalt found in the octahedral sites are diamagnetic (low spin) Co^{3+} [11, 16].

The very intense satellite structure associated with an octahedral, high spin Ni^{2+} is clearly evident in the nickel 2p spectra, however. The satellites features marked as "S" in Figure 4 comprise about 40% of the overall 2p intensity, a value approaching that of NiO crystalline substrates where low-defect surfaces can yield satellites with ≈50% of the total 2p signal. The intense satellite structure is believed to be a direct consequence of the band structure associated with octahedral Ni^{2+} in the oxide lattice, which allows for admixture of oxygen 2p character and leads to two possible final states in the photoemission process:

$$2p^6 3d^8 + h\nu \rightarrow 2p^5 3d^8 + e^- \text{ or } 2p^5 3d^9 \underline{L} + e^-$$

where $\underline{L}$ represents an electron vacancy in the 2p band of the neighboring O^{2-} lattice ions. Because of the extreme
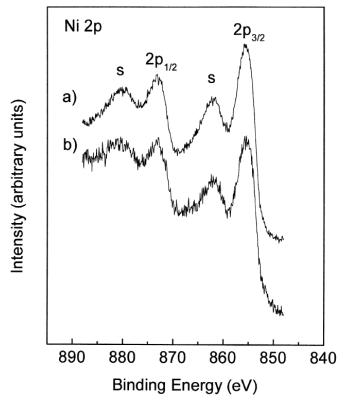

Figure 4. Nickel 2p XPS for (a) thermal decomposition and (b) sol–gel methods.

sensitivity of the charge-transfer process to the overlap between adjacent Ni^{2+} and O^{2-} orbitals, the satellite to main peak intensity is highly dependent upon the geometry and defect nature of the nickel compound. Studies of the NiO valence band suggest the lower binding energy Ni 2p peak is associated with the $2p^5 3d^9 \underline{L}$ state and the satellite feature with the $2p^5 3d^8$ state in the photoemission process [25, 26], although the actual peak assignment is less important for the present purpose than the sensitivity of the spectral structure to chemical environment and lattice structure.

The nickel $2p_{3/2}$ and $2p_{1/2}$ binding energies, at 854.9 and 872.9 eV, respectively, are also comparable to the octahedral Ni^{2+} species found in NiO [20] and are in good agreement with the higher values reported in the literature for $NiCo_2O_4$ [11, 13, 14]. Samples produced by thermal decomposition and by sol–gel methods yield comparable spectra. The full width at half maximum (FWHM) of the $2p_{3/2}$ main peak is 4.2–4.7 eV for spectra taken with a 25-eV band pass. Therefore, the majority of the nickel at the $NiCo_2O_4$ surface is found as Ni^{2+} in octahedral sites.

Oxygen concentrations can also be obtained from XPS data through use of Eq. (2) with integrated O 1s XPS intensities and sensitivity factors. Using $S_{Ni} = 4.5$ and $S_{Co} = 3.8$, as above, and $S_O = 0.48$ [25], the concentration of oxygen is found to be $C_O/C_{Ni}+C_{Co} = 1.31 \pm 0.18$ for the sol–gel and $C_O/C_{Ni}+C_{Co} = 0.96 \pm 0.34$ for the thermal decomposition samples. While these results are in good agreement with concentrations obtained by Auger analysis, the O 1s peak shape (Figure 5) shows that the oxygen region of the photoelectron spectrum, with at least two distinct peaks contributing to the spectrum, is more complicated than might be expected from the single set of equivalent O^{2-} lattice species found in the bulk of the spinel lattice.

Figure 5a shows the O 1s region for a sample of $NiCo_2O_4$ prepared by the thermal decomposition method. The main peak, taken here to have a binding energy of 529.6 eV, has been observed for lattice O^{2-} at approximately this value in a number of rocksalt and spinel 3d metal oxides [20], including CoO [21–24], NiO [25, 27], and Co_3O_4 [21, 28]. A second, higher-binding energy peak is found at 531.2 eV (Figure 5b), and perhaps a third peak at 533.0 eV. The latter peak is only present in about 7% of the total O 1s intensity and may simply be an artifact of fitting asymmetric XPS peaks
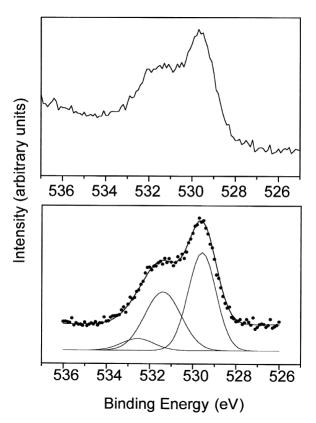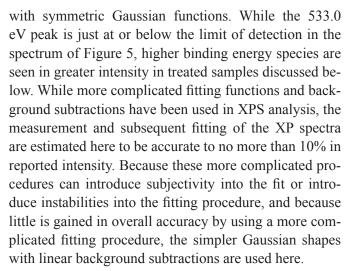
Figure 5. Oxygen 1s XPS (a) for a $NiCo_2O_4$ thermal decomposition sample and (b) the same spectrum with a linear background removed and fit with three Gaussian peaks as shown. In trace (b), the data are represented by circles and the sum of the three Gaussian peaks is shown as a continuous line.

Figure 6. Oxygen 1s XPS for (a) CoO(100), (b) Co_3O_4 and (c) $NiCo_2O_4$.

with symmetric Gaussian functions. While the 533.0 eV peak is just at or below the limit of detection in the spectrum of Figure 5, higher binding energy species are seen in greater intensity in treated samples discussed below. While more complicated fitting functions and background subtractions have been used in XPS analysis, the measurement and subsequent fitting of the XP spectra are estimated here to be accurate to no more than 10% in reported intensity. Because these more complicated procedures can introduce subjectivity into the fit or introduce instabilities into the fitting procedure, and because little is gained in overall accuracy by using a more complicated fitting procedure, the simpler Gaussian shapes with linear background subtractions are used here.

The 531.2-eV peak is characteristic of all prepared $NiCo_2O_4$ samples, but while the binding energy of this peak remains constant to within the error of the measurement, the intensity varies drastically, from 20–75% of the main peak intensity, even for samples that appear to be prepared in similar ways. The average O 1s
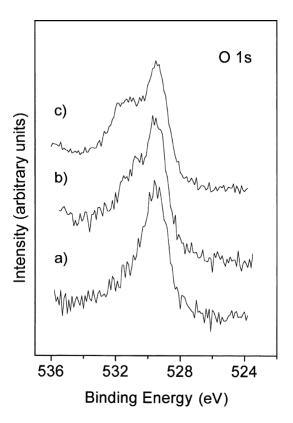
531.2 eV intensity is 30–40% of the 529.6 eV value, and while the thermal decomposition preparations tend to result in slightly smaller 531.2 eV peak intensities than do the sol–gel methods (32% vs. 39% average intensity), the variation within the preparative methods is much greater than between the average values for each of the two methods.

Establishing a unique assignment for the 531.2 eV O 1s peak is, unfortunately, not straightforward. There are several possible defects and contaminants with a comparable XP binding energy and similar peaks in O 1s spectra taken on nickel- and cobalt-containing oxides have been assigned to a variety of surface species including hydroxyls, both those resulting from ambient adsorption and from intrinsic oxyhydroxide compositions [18, 19, 29–31], chemisorbed oxygen [32], under-coordinated lattice oxygen [22], Ni_2O_3/Co_2O_3-like surface phases [24, 33], or species intrinsic to the surface of the spinel [16, 21]. Figure 6 compares XP spectra for the O 1s region of the UHV-cleaved CoO(100) and Co_3O_4 sin-

gle crystal samples, and a typical NiCo$_2$O$_4$ powder sample from these studies. Note the distinct presence of the 531.2-eV satellite peak in the vacuum-cleaved spinel Co$_3$O$_4$ O 1s spectrum. The two oxygen species found in both the UHV-cleaved Co$_3$O$_4$ and the NiCo$_2$O$_4$ spectra match in binding energies although the 531.2 eV/529.6 eV relative intensities tend to be more variable and the peak widths somewhat higher in the NiCo$_2$O$_4$ spectra. Thus, while it is not possible to rule out low levels of contaminants or defect species entirely, a fair percentage of oxygen intensity in the NiCo$_2$O$_4$ O 1s spectrum is believed to be representative of surface oxide intrinsic to the NiCo$_2$O$_4$ spinel lattice.

3.3. Surface reactivity

The NiCo$_2$O$_4$ samples appear stable under UHV, at least on the time scale required of the XPS analysis. However, the sample does decompose when heated. Figure 7 shows the oxygen Auger intensity as a function of sample temperature for NiCo$_2$O$_4$, in this case prepared by the thermal decomposition method. The figure gives both absolute values of integrated Auger intensity for the oxygen KL$_2$L$_2$ peak (Figure 7a) and the oxygen concentration relative to that of the total metal (Figure 7b), calculated from Auger measurements by the method described above. The data do not represent either equilibrium or steady-state concentrations but instead are a slow thermal desorption experiment in which the sample is heated sequentially in 50° steps for 20 min per step between the Auger measurements. The NiCo$_2$O$_4$ remains stable to within the error of the measurement but begins to show significant signs of decomposition through loss of oxygen at approximately 625 K. Throughout the experiment, the Ni/Co atomic ratio remains constant at 1/2 ($x_{surface} = 0.33$).

XP spectra, taken at the beginning and end of the thermal desorption experiment, are compared in Figure 8, Figure 9 and Figure 10, along with spectra taken after the oxygen-depleted surface is heated under 1×10^{-6} Torr O$_2$ at 625 K until the oxygen surface concentration is restored approximately to that of the spinel material (~2 h). The loss in oxygen content upon heating comes primarily at the expense of the 531.2 eV O 1s peak, as seen in Figure 8b, with the 529.6-eV main peak intensity decreasing only slightly during the reduction process.
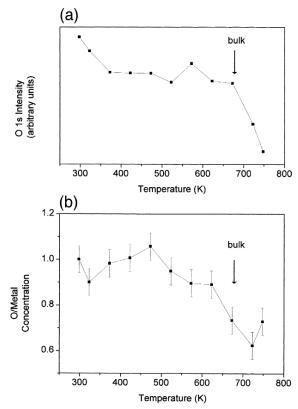

Figure 7. O Auger intensity for NiCo$_2$O$_4$ prepared by thermal decomposition as a function of reduction temperature, as described in the text for (a) absolute integrated intensities and (b) oxygen to total metal atomic ratios calculated by use of Eq. (2). Arrows indicate bulk decomposition observed by TGA-DTA in [15].

Concurrent with the loss of oxygen, the surface becomes enriched with nickel to give a nickel to total metal ratio of $x_{surface} = 0.48$. (Ni/Co~1). However, the nickel 2p spectrum does not change significantly during the surface reduction (Figure 9b), although the spectral features broaden slightly, with some of the broadening occurring to the higher binding energy side of the 2p$_{3/2}$ peak in the vicinity of the 856 eV peak. While the peak was previously associated with Ni(OH)$_2$ or NiOOH formation from ambient water adsorption during the synthesis of the material [11, 13, 14], this does not appear likely, at least in significant amounts, under the present reaction conditions (UHV~3×10^{-10} Torr at 750 K). Other possibilities include the oxidation of Ni^{2+} to Ni^{3+} [37], which is unusual given that the surface is being reduced under UHV but is not entirely impossible if the oxidation of nickel is compensated by an even larger number of co-
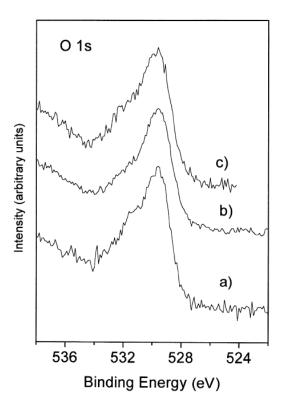
Figure 8. O 1s XPS of (a) a stoichiometric $NiCo_2O_4$ sample, (b) the same sample reduced by heating under UHV to 750 K and (c) the reduced sample of trace b heated under 1×10^{-6} Torr O_2 at 625 K for 2 h.

Figure 9. Nickel 2p XPS of (a) stoichiometric $NiCo_2O_4$, (b) the same sample reduced after heating under UHV to 750 K and (c) the reduced sample of trace b heated under 1×10^{-6} Torr O_2 at 625 K for 2 h. The arrow in trace b points to the 856 eV nickel species that forms on the surface upon reduction.

balt cations reduced from Co^{3+} to Co^{2+}, or the migration of Ni^{2+} to tetrahedral sites [38, 39]. The exact form of this defect-nickel structure cannot be unequivocally determined with XPS, although the structure is clearly associated with a reduced $NiCo_2O_4$ and not with a hydroxylated form of the stoichiometric surface.

The cobalt 2p spectrum changes substantially upon reduction (Figure 10b), and now shows well-developed satellite structure characteristic of high spin octahedral cations, as exhibited by the Co^{2+} metal monoxides. This spectrum also broadens considerably, although in the case of the cobalt the broadening is predominately to the higher binding energy side of the 2p transitions. Thus, the cobalt XPS clearly indicates reduction to octahedrally coordinated Co^{2+} surface species.

Reduction of the $NiCo_2O_4$ surface under UHV is accompanied by the appearance of monoxide-like characteristics in the XP spectra at the expense of those specific to the spinel. However, once the spinel has undergone surface reduction, not all of the changes are completely
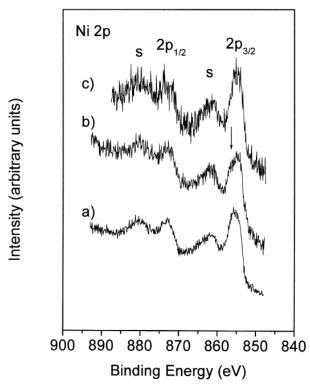
reversed upon re-oxidation. The oxygen concentration of the near-surface can be approximately restored to the spinel atomic ratio of 1.3 O/total metal by heating the substrate under 1×10^{-6} Torr O_2. To perform the re-oxidation, dry O_2 was leaked into the UHV chamber with the turbo pump running. The 531.2 eV O 1s shoulder reforms on the higher binding energy side of the main 529.6 eV lattice peak, and the total oxygen concentration of the surface saturates after about two h under these conditions (Figure 8c: O/M = 1.2). Note that the binding energy and the intensity of the 531.2 eV satellite is approximately that found on the original $NiCo_2O_4$ sample and on the Co_3O_4 UHV-cleaved crystal, even though the $NiCo_2O_4$ surface reduction and subsequent UHV re-oxidation were performed entirely under UHV conditions with no exposure to ambient atmospheric contaminants. Nickel 2p spectra, which merely broadened slightly during the reduction process, re-sharpen to their original $NiCo_2O_4$ peak shape (Figure 9c) during re-oxidation. However, the cobalt 2p spectrum undergoes fur-
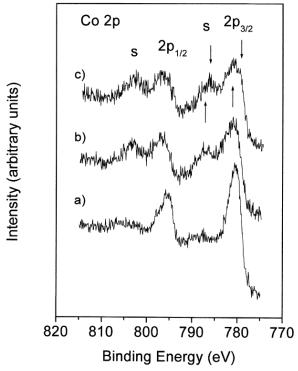
Figure 10. Cobalt 2p XPS of (a) stoichiometric NiCo$_2$O$_4$, (b) the same sample reduced after heating under UHV to 750 K and (c) the reduced sample of trace b heated under 1×10^{-6} Torr O$_2$ at 625 K for 2 h. The arrows in trace c indicate the two sets of cobalt 2p$_{3/2}$ spectra that are found upon phase separation.

Figure 11. O 1s XPS for the reduced NiCo$_2$O$_4$ sample (a) immediately after reduction and after (b) 12 h, (c) 24 h and (d) 48 h under ambient in UHV. The arrows in the upper panel indicate the position of the three Gaussian peaks, which fit the data in the lower panel. The data are represented by circles and the sum of the three Gaussian peaks is shown as a continuous line. A linear background has been subtracted from the data prior to fitting.

ther changes to separate into two distinct sets of cobalt peaks (Figure 10c), one of which is associated with significant satellite structure, as found in the monoxide, and the other of which is comparable to that of the spinel.

Upon oxygen anneal, the reduced surface composition does not return completely to that of the NiCo$_2$O$_4$ spinel in terms of either spectral structure or metal concentration ratios. The cobalt surface concentration increases substantially during the re-oxidation to form 75–80% of the total surface metal content ($x_{surface}$~0.2–0.25). The data are, therefore, consistent with the formation of spinel Co$_3$O$_4$, perhaps doped with small amounts of nickel, and a monoxide Ni$_x$Co$_{1-x}$O surface phase [16].

The reduced NiCo$_2$O$_4$ surface is considerably more reactive to background gases than is that of the as-introduced substrate. Figure 11 shows the O 1s region for XPS of the NiCo$_2$O$_4$ substrate, first reduced by heating the substrate under UHV at 750 K for 0.5 h (Figure 11a), but allowed to remain under UHV for several days

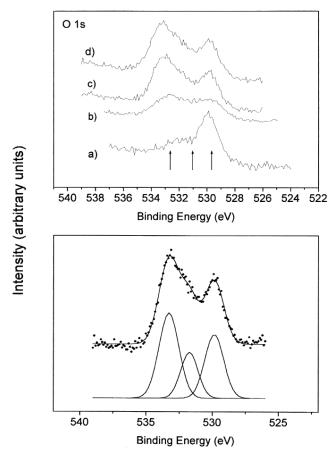with XPS taken in intervals of approximately 24 h (Figure 11b–d). The reduced surface is extremely active to the adsorption of oxygen-containing background gases, which in a stainless steel UHV system will be predominantly water and CO.

There is clearly intensity building in the region of the 531.2 eV spinel peak, which might include contributions from hydroxyl species and some small amount of submonolayer quantities of the background adsorbates undoubtedly do form on the reduced surface. Fitting the O 1s spectrum results in peaks at 529.6, 531.5 and 533.0 eV ($R^2 = 0.988$, FWHM = 1.43, 1.31 and 1.50 eV, respectively). Cobalt and nickel hydroxides [24, 33] have been reported with binding energies of about 531.7 eV,
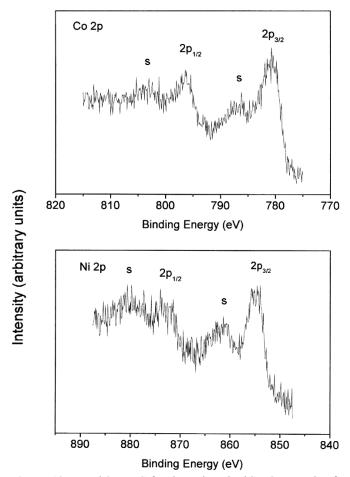
Figure 12. Metal 2p XPS for the reduced $NiCo_2O_4$ sample after 48 h under ambient in UHV.
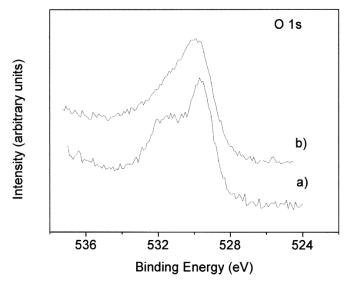

Figure 13. O 1s XPS for (a) the stoichiometric $NiCo_2O_4$ and (b) the stoichiometric sample ultrasonicated in H_2O.

and the slight shift to higher binding energies of the second peak might result from an increased contribution from surface hydroxyls, which adsorb at reduced metal sites to compensate the loss of lattice oxygen. During re-oxidation, the relative 531.5 to 529.6 eV intensity increases from the reduced surface value of approximately 20% for 531.2 eV relative to the 529.6 eV intensity to one ($\sim$40% 531.5 eV relative to 529.6 eV) that is identical within error to that measured for vacuum-cleaved Co_3O_4 single crystals and for the stoichiometric $NiCo_2O_4$ samples.

The greatest contribution from background adsorbates in the O 1s XP spectrum is the 533.0 eV peak seen in Figure 5 above as "residual" after fitting the $NiCo_2O_4$ O 1s spectrum to its main peaks at 529.6 and 531.2 eV due to the spinel lattice. Concomitant with the appearance of the O 1s 533.0 eV peak, carbon is observed with a single peak in the XP spectrum at 285.2 eV, and both O 1s and C 1s binding energies are comparable to values observed for chemisorbed CO on metals [34, 35, 36] and on metal oxides [37]. The new adsorbate peak is at least 1 eV too high in binding energy to result from surface hydroxyls or near-surface oxyhydroxide formation due to background water adsorption, although the binding energy is not unreasonable for molecularly adsorbed water.

Metal concentrations and peak shapes do not change significantly as a result of background gas adsorption, although the 2p metal peaks sharpen somewhat (Figure 12), perhaps as background gas adsorption compensates for non-stoichiometries and defects produced in the near-surface region during the reduction process. However, the primary form of the metals remains monoxide-like on both reduced and re-oxidized $NiCo_2O_4$ samples.

Adsorption of water onto the stoichiometric $NiCo_2O_4$ surface is actually quite slow under UHV conditions and the amount of surface hydroxylation that occurs at these low partial pressure of water ($P_{H2}O \lesssim 10^{-10}$ Torr) is difficult to separate from the spinel oxide 531.2 eV peak. Stoichiometric $NiCo_2O_4$ samples that were ultrasonicated in H_2O prior to their admission to UHV for surface analysis did show evidence of hydroxyl formation in the broadening of the O 1s spectrum and present a very different peak shape than do the stoichiometric $NiCo_2O_4$ samples (Figure 13). However, the 2p spectra were not significantly different from that of stoichiometric sam-

ples that were placed into UHV within minutes of their preparation. The nickel 2p spectrum also retained the peak shape and satellite structure observed for untreated, stoichiometric NiCo$_2$O$_4$ surfaces (Figure 14), with no indication of Ni(OH)$_2$, which would be expected to give a higher binding energy 2p$_{3/2}$ peak at about 856 eV [33]. NiOOH-like surface phases are more difficult to rule out because of the similarity in binding energies and peak shape structure for the Ni^{2+}cation [33].

There is a slight change to the cobalt 2p satellite structure and 2p peak widths for the ultrasonicated sample; however, the spectrum remains quite close to that of the stoichiometric NiCo$_2$O$_4$ spinel. Again, while some surface hydroxylation associated with cobalt sites cannot be ruled out, there is no evidence of Co(OH)$_2$ formation at the surface of the water-treated samples. Similarly CoOOH, if it forms, does so in very small quantities since the satellite peak shape structure of the oxyhydroxide is similar to that found on CoO [24]. Thus, the changes that were observed for the metal 2p XPS for reduction and reoxidation under UHV conditions are unlikely to be due to surface hydroxylation or oxyhydroxide formation. The primary source of these changes is phase separation due to the formation of monoxide-like surface oxides.

Figure 14. Metal 2p XPS for NiCo$_2$O$_4$ ultrasonicated in H$_2$O.

4. Discussion

Mixed-metal transition oxides have been the subject of a number of recent surface analytical studies, and many of these reports focus on metal oxidation states and hydroxyl formation. For studies in which XPS plays a significant role, the formation of hydroxyls and oxyhydroxide surface phases is treated as a forgone conclusion and peak-fitting routines are used to generate components in line with this assumption. Unfortunately, the assignment is not unique and other assumptions, if perceived to be valid, could lead to significantly different but equally reasonable conclusions on the near-surface composition.

There is no question that hydroxylation represents a ubiquitous phenomenon for oxide surfaces, and oxide samples exposed to ambient atmosphere have long been known to show signs of surface hydroxylation [40, 41, 42]. However, the changes that occur with surface hydroxylation are perhaps more subtle than often assumed
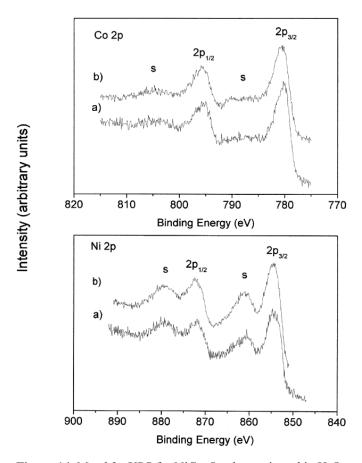
in interpreting XPS data and a more controlling feature of surface composition in mixed-metal oxides may be due to oxidation/reduction effects and phase separation during the materials synthesis process. This is the case for as-fabricated NiCo$_2$O$_4$ samples, where irreversible phase separation into Co$_3$O$_4$-like spinel and NiO/CoO rocksalt metal monoxide is observed at the substrate surface upon UHV-reduction and subsequent attempts at reoxidation.

Synthesizing the NiCo$_2$O$_4$ material, whether by sol–gel or thermal decomposition methods, requires a careful balance of preparation time and temperature with other reaction conditions. The reaction must be heated to a high enough temperature for sufficiently long to decompose the reactants and allow for complete inter-diffusion of the reacting materials; the temperature must also be low enough and the reaction time short enough so that the desired spinel does not lose oxygen to make

it severely non-stoichiometric or create phase separation through partial decomposition of one or both components into lower oxide species. Treatments that yield homogeneous materials by XRD and other bulk methods often leave the surface oxygen-deficient, increasing the reactivity toward water and other ambient gases and creating phase separation of monoxide-like materials. Once they have formed, it is not possible to reoxidize the material and regenerate the original stoichiometric and homogeneous spinel.

The present studies show that it is possible to synthesize $NiCo_2O_4$ that is both bulk and surface homogeneous. Sol–gel and thermal decomposition techniques can both be used to produce surfaces with bulk-like compositions, although the thermal decomposition method tends to produce surfaces that are slightly oxygen-deficient. There is some variability in oxygen content of samples produced by either method, however, and it is difficult to estimate the surface hydroxylation by XPS due to overlap with other surface oxide features.

The as-introduced $NiCo_2O_4$ sample contains similar nickel to cobalt ratios at the surface as in the bulk, as estimated by both Auger and XPS techniques. XPS indicates that at the surface the nickel is present predominately as octahedral Ni^{2+} whereas the cobalt has little or no octahedral Co^{2+}. Thus, the sample surface is most typically represented by the formula $Co^{3+}[Ni^{2+},Co^{3+}]O_4$, where cations before the brackets are placed into tetrahedral sites and those within brackets are placed into octahedral sites. Small deviations from this formula, on the order of 10–15%, cannot be ruled out, although we choose not to attempt to fit the metal 2p XP spectra to identify species present at this level due to the complex and highly variable nature of the satellite structure of these peaks.

The O 1s XP spectrum of the as-introduced $NiCo_2O_4$ sample is more complicated than the one-component, one peak spectrum typical of most late 3d transition metal oxides, with a "lattice peak" at 529.6 eV in agreement with the lattice O^{2-} and a second peak, found here at 531.2 eV and in other studies at comparable values. Because all lattice oxygen are equivalent in the spinel lattice, the appearance of this second peak has been routinely assigned to surface hydroxyls in most recent analyses of the mixed-metal oxide surface. We believe that a large component of this peak is due to intrinsic spinel surface oxide and that the majority of the 531.2 eV component shown for the near-stoichiometric $NiCo_2O_4$ sample (Figure 5) is intrinsic to the spinel surface and not a result of surface hydroxylation or oxyhydroxide formation. The 531.2 eV peak is not correlated with the 856 eV peak reported elsewhere and assigned to surface oxyhydroxides.

Similar high-binding energy O 1s peaks have been found for UHV studies of low P_{O2}-oxidized cobalt metal [43] and cobalt monoxide [21] substrates, $Ni_xCo_{1-x}O$ solid solutions [16], $Mn_xCo_{3-x}O_4$ solid solutions [29 and 44], $La_{0.65}A_{0.35}MnO_3$ (A = Ca, Sr, Ba) giant magnetoresistance thin films [45] and Co_3O_4 single crystals cracked to produce a fresh surface under UHV (Figure 6b). In addition to hydroxyl contamination resulting even from low pressure H_2O background contaminants from the UHV chamber, the peak has been proposed to result from non-stoichiometric near-surface oxygen [24, 46], cation defects in spinel-like near-surface layers [21, 44], phases resulting from surface segregation of one bulk metal component along with increased oxidation of the near-surface region [29], a final-state effect intrinsic to the spinel surface [47] and even a residual substrate signal from the oxide upon which the spinel was grown [29]. The very intense nature indicates that the peak is characteristic of a species that is more than simply a casual contaminant that formed on the outermost layer from UHV ambient absorption.

Heating the $NiCo_2O_4$ sample in UHV causes the surface to lose oxygen as expected, although the temperature at which surface oxygen loss becomes rapid (~625 K) is significantly lower than the value (723 K) at which bulk decomposition is first reported [15]. The conditions are, of course, significantly different but the point remains that surface decomposition can occur well before it is detected by bulk measurement and that this decomposition can lead to the irreversible formation of other oxide phases. Because the surface is more reactive in its reduced form, reaction with ambient gases can easily occur and since these reactions will be specific to the ambient contaminants present they will lead to a wide range of poorly reproduced surface compositions. Once reduced, for example, reoxidation causes an irreversible phase separation into Co_3O_4 and $Ni_xCo_{1-x}O$. During the surface reactions, the cobalt exhibits a wider range

of chemical nature, as followed by XPS, than does the nickel, which remains largely octahedrally coordinated Ni^{2+} throughout the present studies.

Note that in the present studies, the NiCo$_2$O$_4$ samples were not investigated for their electrocatalytic properties or under conditions that approximate reaction environments during electrocatalysis. Rather, the focus is on the surface composition and reactivity of as-synthesized nickel cobaltite materials. Substrates undergoing electrocatalytic processes, particularly those occurring in aqueous media, are bound to be more heavily hydroxylated than the present nickel cobaltite materials, and the hydroxyls that form are no doubt influential if not crucial to the mechanistic behavior of metal oxide substrates under these circumstances. The present studies are not meant to deny this importance. Rather, the results here elucidate how substrate synthesis and conditioning treatment can create phase separation or otherwise change the nature of the material irreversibly. The small differences in surface oxygen content found between NiCo$_2$O$_4$ samples prepared by thermal decomposition and sol–gel methods probably do not persist for a significant amount of time into the electrocatalysis. Oxide defects do serve as adsorption sites for reactants in redox reactions, but these defects are most likely easily formed and annihilated repeatedly during the reaction. However, the defects might affect the rate at which stored substrates react with the ambient, to form carbonates for example, and therefore, might influence the storage and aging properties of the cobaltite materials. These speculations must await further studies specifically designed to answer such questions.

5. Conclusion

Powder NiCo$_2$O$_4$ samples have been fabricated by sol–gel and thermal decomposition methods and analyzed by Auger and XPS surface-sensitive techniques. The as-introduced samples are found to be near-stoichiometric, with metal concentrations within error of that found in the bulk, although the thermal decomposition samples are slightly reduced in oxygen concentration. Nickel surface cations are predominately present as octahedrally coordinated Ni^{2+} and the cobalt are divided between tetrahedral and octahedral sites approximately equally. The lack of characteristic satellite

structure in the cobalt 2p spectrum identifies the spinel formula as Co^{3+}[Ni^{2+},Co^{3+}]O$_4$. The oxygen 1s spectrum is comprised of two peaks: one at 529.6 eV, similar to that found for lattice O^{2-} in the monoxides, and a second at 531.2 eV, which we believe to be characteristic of the surface spinel. The relative intensity is 60% 529.6 eV/40% 531.2 eV, although this ratio is somewhat variable and might also contain unresolved contributions from surface hydroxyls and oxyhydroxides.

Reduced surfaces show signs of nickel segregation as metal monoxide, along with a substantial change in the cobalt chemical state. Reoxidation causes phase separation into Co$_3$O$_4$, perhaps with some Ni^{2+} dissolved in the spinel lattice, and metal monoxide most likely found as the solid solution Ni$_x$Co$_{1-x}$O, since the monoxides are known to dissolve in each other in all proportions. While the reduced surface is considerably more reactive than stoichiometric NiCo$_2$O$_4$, adsorption of water either from the ambient or from ultrasonication in liquid H$_2$O, did not cause substantial changes in the XP spectra of either metal and only caused a broadening of the O 1s spectrum, indicating that hydroxylation effects are subtle and are difficult to separate from intrinsic features of the NiCo$_2$O$_4$ surface.

References

1. S. Trasatti. In: J. Lipkowski and P.N. Ross, Editors, *The Electrochemistry of Novel Materials*, VCH, New York (1994).
2. K. Kinoshita. *Electrical Oxygen Technology*, Wiley, New York (1994) The Electrochemical Society Series.
3. S. Holgersson and A. Karlsson. *Z. Anorg. Allg. Chem.* **183** (1929), p. 384.
4. M. Lenglet, R. Guillamet, J. Durr, D. Gray and R.E. Vandenberghe. *Solid State Commun.* **74** (1990), p. 1035.
5. G. Blasse. *Philips Res. Rep.* **18** (1963), p. 383.
6. D. Mehanjiev and E. Nikolova-Zhencheva. *Thermochemica Acta* **51** (1981), p. 343.
7. O. Knop, K.I.G. Reid, Sutarno and Y. Nakagawa. *Can. J. Chem.* **46** (1968), p. 3463.

8. W.J. King and A.C. Tseung. *Electrochim. Acta* **19** (1974), p. 493.

9. P.D. Battle, A.K. Cheetham and J.B. Goodenough. *Mater. Res. Bull.* **14** (1979), p. 1013.

10. D. Pyke, K.K. Mallick, R. Reynolds and A.K. Bhattacharya. *J. Mater. Chem.* **8** (1998), p. 1095.

11. Yu.E. Roginskaya, O.V. Morozova, E.N. Lubnin, Yu.E. Ulitina, G.V. Lopukhova and S. Trasatti. *Langmuir* **13** (1997), p. 4621.

12. M. Lenglet, A. D'Huysser and J. Durr. *Annales de Chimie-Science des Materiaux* **13** (1988), p. 505 and references therein.

13. A.C. Tavares, M.A.M. Cartaxo, M.I. da Silva Pereira and F.M. Costa. *J. Electroanal. Chem.* **464** (1999), p. 187.

14. A.C. Tavares, M.I. da Silva Pereira, M.H. Mendonca, M.R. Nunes, F.M. Costa and C.M. Sa. *J. Electroanal. Chem.* **449** (1998), p. 91.

15. M. ElBaydi, S.K. Tiwari, R.N. Singh, J.L. Rehspringer, P. Chartier, J.F. Koenig and G. Poillerat. *J. Solid State Chem.* **116** (1995), p. 157.

16. M.W. Nydegger, G. Couderc and M.A. Langell. *Appl. Surf. Sci.* **147** (1999), p. 58.

17. S. Mroczkowski and D. Lichtman. *Surf. Sci.* **127** (1983), p. 121.

18. S. Mroczowski and D. Lichtman. *Surf. Sci.* **131** (1983), p. 159.

19. L.E. Davis, N.C. MacDonald, P.W. Palmberg, G.E. Riach, R.E. Weber, Handbook of Auger Electron Spectroscopy, Physical Electronics Industries, Eden Prairie, 1976, pp. 89 and 93.

20. D. Briggs and M.P. Seah. *Practical Surface Analysis*, Wiley, New York (1990).

21. G.A. Carson, M.H. Nassir and M.A. Langell. *J. Vac. Sci. Technol.* **14** (1996), p. 9006.

22. V.M. Jimenez, A. Fernandez, J.P. Espinos and A.R. Gonzales-Elipe. *J. Electron Spectrosc. Relat. Phenom.* **71** (1995), p. 61.

23. B. Marcus-Saubat, J.P. Beaufils and Y. Barbaux. *J. Chim. Phys.* **83** (1986), p. 317.

24. C.R. Brundle, T.J. Chuang and D.W. Rice. *Surf. Sci.* **60** (1976), p. 286.

25. Z.-X. Shen, C.K. Shih, O. Jepsen, W.E. Spicer, I. Lindeau and J.W. Allen. *Phys. Rev. Lett.* **64** (1990), p. 2442.

26. A. Fujimori and F. Minami. *Phys. Rev. B* **30** (1984), p. 957.

27. K. Wulser and M.A. Langell. *Catal. Lett.* **15** (1992), p. 39.

28. M.A. Langell, G.A. Carson, M. Anderson, S. Smith and L. Peng. *Phys. Rev. B* **59** (1999), p. 4791.

29. J.L. Gautier, E. Rios, M. Garcia, J.F. Marco and J.R. Gancedo. *Thin Solid Films* **311** (1997), p. 51.

30. H.W. Nesbitt and D. Banerjee. *American Mineralogist* **83** (1998), p. 305.

31. B. Klingenberg, F. Grellner, D. Borgmann and G. Wedler. *Surf. Sci.* **383** (1997), p. 13.

32. J. Lahtinen, J. Vaari, A. Talo, A. Vehanen and P. Hautojarvi. *Vacuum* **41** (1990), p. 112.

33. K.S. Kim and N. Winograd. *Surf. Sci.* **43** (1974), p. 625.

34. F. Zaera. *J. Vac. Sci. Technol., A* **7** (1989), p. 640.

35. T. Asakawa, K. Tanaka and I. Toyoshima. *J. Phys. Chem.* **95** (1991), p. 4783.

36. P.R. Norton, R.T. Tapping and J.W. Goodale. *Chem. Phys. Lett.* **41** (1976), p. 247.

37. T. Hashemi and A.W. Brinkman. *J. Mater. Res.* **7** (1992), p. 1278.

38. G.C. Allen, S.J. Harris, J.A. Jutson and J.M. Dyke. *Appl. Surf. Sci.* **37** (1989), p. 111.

39. L. Salvati, L.E. Makovsky, J.M. Stencel, F.R. Brown and D.M. Hercules. *J. Phys. Chem.* **85** (1981), p. 3700.

40. N.G. Yaroslavskii and A.N. Terenin. *Dokl. Akad. Nauk. SSSR* **66** (1949), p. 835.

41. R.P. Eischens and W.A. Pliskin. *Adv. Catal.* **10** (1958), p. 1.

42. L.H. Little. *Infrared Spectroscopy of Adsorbed Species*, Academic Press, New York (1966) and references contained therein.

43. M. Oku and Y. Sato. *Appl. Surf. Sci.* **55** (1992), p. 37.

44. M.A. Langell, F. Gevrey and M.W. Nydegger. *Appl. Surf. Sci.* **153** (2000), p. 114.

45. J.-W. Choi, H. Dulli, Y. Feng, S.-H. Liou, P.A. Dowben and M.A. Langell. *Phys. Status Solidi B* **214** (1999), p. 45.

46. S. Ching, D.J. Petrovay and S. Suib. *Inorg. Chem.* **36** (1997), p. 883.

47. S.A. Chambers and S.A. Joyce. *Surf. Sci.* **420** (1999), p. 111.